Transportation Research Part C 114 (2020) 504–516

Contents lists available at ScienceDirect

Transportation Research Part C

journal homepage: www.elsevier.com/locate/trc

A two-dimensional car-following model for two-dimensional traffic flow problems☆

Rafael Delpiano[a,*], Juan Carlos Herrera[b], Jorge Laval[c], Juan Enrique Coeymans[b]

[a] Facultad de Ingeniería y Ciencias Aplicadas, Universidad de los Andes, Chile, Mons. Álvaro del Portillo 12455, Las Condes, Santiago, Chile
[b] Department of Transport Engineering and Logistics, Pontificia Universidad Católica de Chile, Av. Vicuña Mackenna 4860, Macul Santiago, Chile
[c] School of Civil and Environmental Engineering, Georgia Institute of Technology, Mason Building, 790 Atlantic Drive, Atlanta, GA 30332, USA

ARTICLE INFO

Keywords:
Traffic flow theory
Microscopic traffic models
Car following
Social forces
Two-dimensional traffic
Relaxation phenomenon

ABSTRACT

This paper proposes a two-dimensional car-following model to tackle traffic flow problems where considering continuum lateral distances enables a simpler or more natural mathematical formulation compared to traditional car-following models. These problems include (i) the effects of lateral friction often observed in HOV lanes and diverge bottlenecks, (ii) the relaxation phenomenon at merge bottlenecks, (iii) the occurrence of accidents due to lane changing, and (iv) traffic models for autonomous vehicles (AVs). We conjecture that traditional car-following models, where the lateral dimension is discretized into lanes, struggle with these problems and one has to resort to ad-hoc rules conceived to directly achieve the desired effect, and that are difficult to validate.

We argue that the distance maintained by drivers in order to avoid collisions in all directions plays a fundamental role in all these problems. To test this hypothesis, we propose a simple two-dimensional microscopic car-following model based on the social force paradigm, and build simulation experiments that reproduce these phenomena. These phenomena are reproduced as an indirect consequence of the model's formulation, as opposed to ad-hoc rules, thus shedding light on their causes.

A better understanding of the behavior of human drivers in the lateral dimension can be translated to improving autonomous driving algorithms so that they are human-friendly. In addition, since AV technology is proprietary, we argue that the proposed model should provide a good starting point for building AV traffic flow models when real data becomes available, as these data come from sensors that cover two-dimensional regions.

1. Introduction

Two-dimensional (2D) models for traffic flow have not been used widely in the transportation field. The logic behind a single dimension is simplicity, and that little is lost when discretizing the lateral dimension into lanes. However, there are several key aspects of driving that involve the lateral dimension. We conjecture that some of these aspects are better handled including a continuum lateral dimension, for example: (*i*) the lateral friction often observed in HOV lanes, (*ii*) the relaxation phenomenon near congested merge bottlenecks, (*iii*) accidents due to lane changing, and (*iv*) traffic flow models for autonomous vehicles (AVs). Each of

☆ This article belongs to the Virtual Special Issue on "Traffic flow modeling".

* Corresponding author.
E-mail addresses: rdelpiano@uandes.cl (R. Delpiano), jch@ing.puc.cl (J.C. Herrera), jorge.laval@ce.gatech.edu (J. Laval), jec@ing.puc.cl (J.E. Coeymans).

https://doi.org/10.1016/j.trc.2020.02.025
Received 16 December 2018; Received in revised form 11 February 2020; Accepted 20 February 2020
Available online 02 March 2020
0968-090X/

these aspects will be discussed next.

Lateral friction happens when drivers tend to reduce their speed based on traffic and/or objects adjacent to their traveling lane. The phenomenon was first documented by Case et al. (1953) and has since been a fertile field of research. Lane speed and capacity are influenced by width (Case et al., 1953; Chitturi and Benekohal, 2005) and by neighboring objects: either vehicles on adjacent lanes (May, 1959) or signs, barriers, and the like on the shoulder (Taragin, 1955; Calvi, 2015). Current models address this phenomenon, albeit unsatisfactorily, through *ad-hoc* rules such as imposing a maximum speed difference between lanes (TSS, 2010) or in the reduced field of non-lane-based traffic only (Gunay, 2007; Jin et al., 2010, 2011). With 2D models, no *ad-hoc* rules are needed because friction can be reproduced by natural 2D mechanisms.

Relaxation is the phenomenon by which drivers are willing to accept very small spacing entering a mainline stream and then gradually increase their spacing to comfortable/equilibrium levels. Again, existing models need ad-hoc rules to capture this, either for the lane-changing decision (Gipps, 1986; Treiber et al., 2000; Delpiano et al., 2015) or the car-following model (Laval and Leclercq, 2008). We conjecture that the very small spacings reported in the literature may have been observed when both vehicles were not yet aligned longitudinally. This is consistent with staggered car following, in which drivers accept shorter spacings provided there exists a lateral offset between them (Gunay, 2007).

Accidents due to lane changing are very common, yet current models do not offer the framework to model this process realistically. Again, existing 1D models have been extended with *ad-hoc* rules to capture lane-changing execution as a non-instantaneous process (Moridpour et al., 2010; Yang et al., 2016). Two-dimensional models have the ability to incorporate, for example, the reaction of the driver in the target lane when perceiving a potentially dangerous maneuver in her vicinity. Importantly, this can be especially helpful in the context of AVs: only 2 out of the 38 crashes reported by Google/Waymo in compliance to the California autonomous vehicles testing regulations as of October 2018, involve the vehicle in autonomous mode, moving, and not rear-ended by a third-party vehicle. Both of them were lateral collisions where one of the vehicles entered the other vehicle's lane (California Department of Motor Vehicles, 2018). Therefore, 2D models become relevant for a better understanding of lane-changing execution for both regular and autonomous vehicles.

This second dimension might be also crucial for the development of realistic microscopic traffic flow models for longitudinal and lateral control for AVs. Existing AV car-following models might have serious limitations because none have been based on real AV data (Van Arem et al., 2006; Shladover et al., 2012; Talebpour and Mahmassani, 2016; Mahmassani, 2016; Talebpour et al., 2017; Van Arem et al., 2006; Reece and Shafer, 1993; Kesting et al., 2008; Chen et al., 2017; Ghiasi et al., 2017; Delis et al., 2015). The only exception is Shladover et al. (2012) in the context of adaptive cruise control vehicles, but no details have been published about the model used. To make things worse, AV technology is proprietary and therefore models based on emulating their control logic are usually based on theoretical developments only. The best alternative is to construct such models from real data as they become available. As illustrated in Fig. 1, these data come from sensors that cover two-dimensional regions, and therefore the natural framework for such models is 2D. For a review on the different approaches for AV control coming from the field of robotics, see Katrakazas et al. (2015).

This paper shows that all the above aspects related to driving and AVs can be captured with the family of 2D models proposed

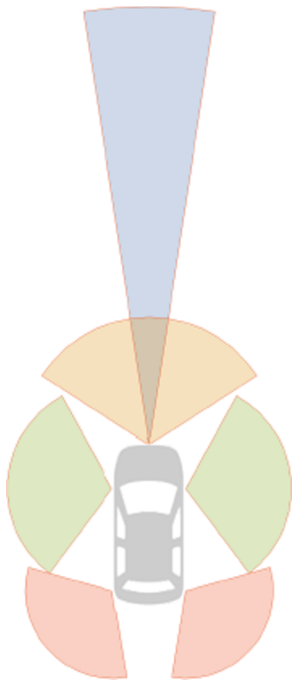

Fig. 1. Simplified schematics of the typical sensing areas of an AV.

here, which is an extension of the 1D model previously reported in Delpiano et al. (2015). The model follows the paradigm of *social* or *generalized* forces (Helbing and Molnár, 1995; Helbing and Tilch, 1998), in which driver behavior is formulated as forces to which vehicles are subject.

Note that 2D models have been reported in the literature before (Gunay, 2007; Jin et al., 2010, 2011; Maurya, 2011; Schönauer et al., 2012; Kanagaraj and Treiber, 2018). However, most of the existing 2D microscopic traffic models were developed for non-lane-based traffic, where the modeling of decisions involving lateral position, if exists, is not influenced by the existence of lanes. A good lateral control strategy for autonomous trucks, in turn, has been theorized favorable for pavement durability (Chen et al., 2019).

Initial trust and perceived risk are crucial for AV technology adoption (Zhang et al., 2019, 2020). It is difficult to separate perceived risk from comfort, and a number of aspects of comfort in automated driving have been studied, including lane-changes (Bellem et al., 2018). However, there is still need for a deeper understanding of comfort in the lateral dimension, for example, in the relation between neighboring vehicles. There is a trade-off between comfort and capacity in a number of situations (Le Vine et al., 2015), but discomfort may also affect capacity negatively through lateral friction (Gunay, 2007; Liu et al., 2011) among other means.

The remainder of this paper is organized as follows: Section 2 presents the proposed family of model. Section 3 details a particular implementation of the model, as well as the experiments aimed at applying it to lateral friction. Section 4 explains the experiments dealing with relaxation and anticipation. Section 5 elaborates on the experiments concerned with lateral collision avoidance by autonomous vehicles. Finally, Section 6 draws the main conclusions of this work, as well as ideas for future research.

2. The model

2.1. Proposed mechanisms for lateral friction and anticipation

In this section we describe the physical mechanism that motivates the proposed model. The key is the multi-directional collision avoidance behavior of drivers, here modeled as a two-dimensional repulsive force between vehicles.

We define three forces acting on each vehicle: The *acceleration* force $\vec{f}^{a}$ representing the driver's willingness to accelerate, the *lane* force $\vec{f}^{l}$ to reproduce the tendency to center in a specific lane, and the *repulsive* force $\vec{f}^{r}$ for collision-avoidance.

Fig. 2 shows simplified schematics of the relevant forces for vehicles in two situations of interest: lateral friction, as in Fig. 2a and b, and aggressive lane-changing, as in Fig. 2c and d.

Regarding lateral friction, as a vehicle in the fast lane overtakes those in the slow lane, the vehicle constantly perceives a repulsive force from some of them, as sketched in Fig. 2a, where the left lane represents faster traffic. The sum of the lateral components of the repulsive forces moves the vehicle away from the center of the lane, which increases the magnitude of the lane force in the opposite direction. Eventually, these two forces become equal. At the same time, the longitudinal component of the repulsive force makes the vehicle to slow down, reducing the magnitude of the repulsive force while increasing the acceleration force, until reaching equilibrium (Fig. 2b).

The proposed mechanism for aggressive lane-changing is the following: soon after a lane-changing vehicle starts displacing laterally, the follower-to-be perceives a stronger repulsive force; see Fig. 2c. Even before the lane-changing vehicle enters the target lane, its new follower is forced to concede some gap (anticipation), to prevent collision. Even in extremely aggressive cases in which both vehicles could end up side by side in the same lane, the model ensures the situation will not last long, since one of the vehicles will perceive a strong repulsive force away from the other, forcing it to give way and slow down as suggested in Fig. 2d. The lateral component of this force will eventually cancel out the lane force, and the vehicle will stay at a lower speed until settling behind.

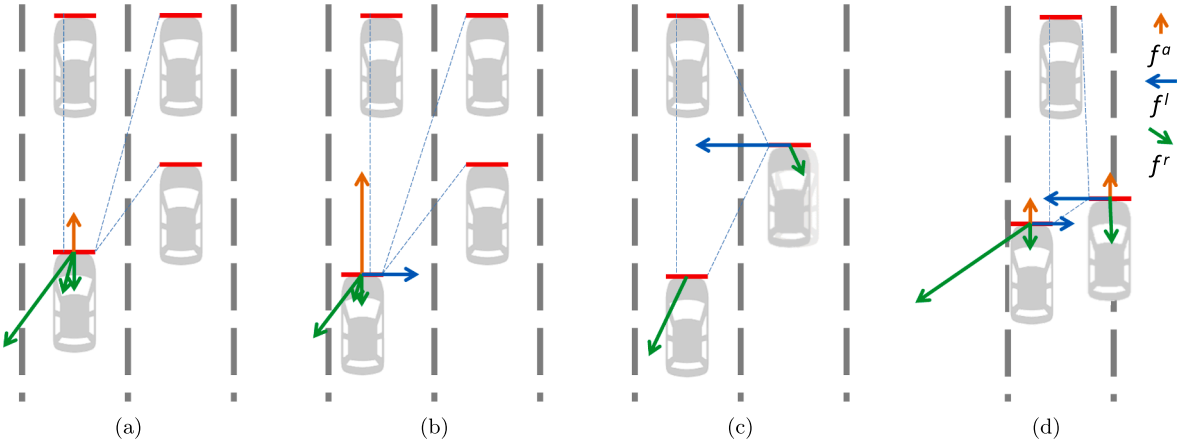

Fig. 2. Simplified schematics of forces involved in specific situations of interest: (a) and (b) deal with the mechanism proposed for lateral friction. In (a), follower in left lane is in equilibrium if it were not for presence of slower vehicles in right lane inducing repulsive forces. In (b), follower in fast lane reaches new equilibrium off-center and at slower speed. (c) shows most relevant forces soon after lane-changing maneuver begins, causing anticipation in the follower-to-be. (d) illustrates resolution mechanism for extreme cases of lateral proximity.

2.2. Original one-dimensional model

Our starting point is the social-force 1D model in (Delpiano et al., 2015). The model is a particular case and formulation of a linear model (Helly, 1959) with bounded acceleration by Tampère (2004). The acceleration of vehicle i at time t can be modeled as the sum of two forces: the acceleration force $f_i^a(t)$ and the interaction or repulsive force $f_i^r(t)$ (see Eq. 1).

$$\begin{aligned}\dot{v}_i(t) &= f_i^a(t) + f_i^r(t) \\ &= (V - v_i(t))c_1 + \min\{0, (v_{i-1}(t) - v_i(t))c_2 + (y_{i-1}(t) - y_i(t) - \tau_r v_i(t) - s_r)c_3\},\end{aligned} \tag{1}$$

where $v_i(t)$ and $v_{i-1}(t)$ are the speeds of vehicle i and its leader $i-1$, while $y_i(t)$ is the (longitudinal) position of vehicle i at time t. The c_1, c_2, c_3, V, τ_r, and s_r are the parameters of the model.

The acceleration force $f_i^a(t)$ reflects the tendency of drivers to accelerate to their desired speed, which is defined as proportional to the difference between the current speed and the maximum desired speed V. The repulsive force $f_i^r(t)$ depends exclusively on the dynamics of the subject vehicle i and its leader, and it becomes active only when vehicle i is approaching or already near to its leading vehicle. In the model, this force grows linearly with the approaching speed and with vehicle spacing.

Parameter c_1 drives the intensity of the acceleration. Parameters c_2 and c_3 adjust the vehicle's sensitivity to differences in speed and deviation from the ideal distance to the preceding vehicle, respectively. V represents the maximum desired (i.e., free-flow) speed. Finally, the meanings of τ_r and s_r are less obvious: $\tau_r v_i(t) + s_r$ is a theoretical equilibrium spacing if there is no acceleration force. Parameter s_r is a distance always greater than jam spacing.

This model allows for the determination of exact trajectories with finite accelerations and decelerations. As traffic tends to equilibrium, the corresponding fundamental diagram becomes triangular. Note that reaction time is implicit in the model's formulation, as is the case with other ODE-based car-following models, such as the OVM (Bando et al., 1995) or the IDM (Treiber et al., 2000). In fact, the model's inherent stability properties allow it to reproduce propagation and amplification of perturbations that lead to stop-and-go waves, provided that condition (2) is met, which is the case when considering realistic values for the parameters.

$$\frac{1}{2}(c_1 + c_3\tau_r)^2 - c_3 + c_2(c_1 + c_3\tau_r) < 0 \tag{2}$$

Fig. 3 exhibits sample trajectories generated by the original model showing stop-and-go behavior resulting from an uphill road.

2.3. The proposed two-dimensional model

The proposed model is a natural two-dimensional generalization of the model presented in previous section. To work in two dimensions (2D) we use 2D vectors as well as 2×2 matrices. We define the lateral dimension as the first dimension (x, and $\hat{\imath}$ the canonical lateral direction vector, whose value grows rightward from the driver's point of view). Hence, the longitudinal dimension is the second one (y, and $\hat{\jmath}$ the canonical longitudinal direction vector).

2.3.1. Acceleration force

The acceleration force $f_i^a(t)$ is mostly longitudinal. For simplicity, we use a longitudinal-only definition:

$$\vec{f}_i^{\,a}(t) = \begin{bmatrix} 0 \\ g_a(v_i^y(t)) \end{bmatrix}, \tag{3}$$

In (3), function g_a provides the magnitude of the longitudinal acceleration aimed at reaching free-flow speed, depending on the current speed in the same axis.

2.3.2. Repulsive force

The repulsive force accounts for the tendency of drivers to avoid collisions. It needs to be two-dimensional to consider not only the leader but also other nearby vehicles that could pose a potential danger when moving laterally. Note that a vehicle may have more than one neighbor repelling it (e.g., from adjacent lanes).

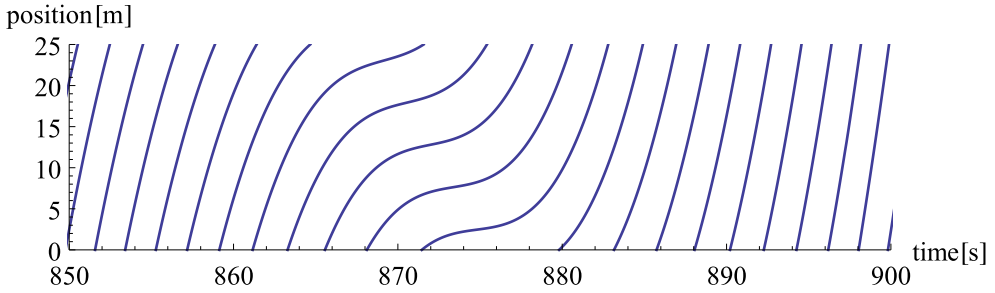

Fig. 3. Sample stop-and-go wave trajectories generated by the social force 1D model.
Source: Delpiano et al. (2015), fig. 7

The repulsive force has to be a response to relative speed and vector distance between vehicles i and k. Let E be the set of vehicles downstream vehicle i and within reach, including adjacent lanes. The total 2D repulsive force exerted over vehicle i is defined as the sum of the repulsive forces over vehicle i generated by each vehicle in the set E:

$$\vec{f}_i^{\,r}(t) = \sum_{k \in E} \vec{f}_{i,k}^{\,r}(t), \tag{4}$$

$$\vec{f}_{i,k}^{\,r}(t) = \vec{g}_r(\vec{v}_k(t), \vec{v}_i(t), \vec{x}_k(t), \vec{x}_i(t)), \tag{5}$$

In (5), vector function $\vec{g}_r$ provides the magnitude of the acceleration in both axes induced in vehicle i by a repelling vehicle k. Vectors $\vec{v}_k(t)$, $\vec{v}_i(t)$, $\vec{x}_k(t)$, and $\vec{x}_i(t)$ are, respectively, the 2D velocities of vehicles k and i, and their positions.

2.3.3. Lane force

The lane force $f_i^l(t)$ aims to keep vehicles close to the center of the lane, countering the effect of the repulsive force from neighboring lanes. It should be a function of the vehicle's lateral speed and its lateral distance to the center of the lane.

If x_l is the lateral position of the center of lane l, the lane force is defined as follows:

$$\vec{f}_i^{\,l}(t) = \begin{bmatrix} g_l(v_i^x(t), x_i(t) - x_l) \\ 0 \end{bmatrix}, \tag{6}$$

In (6), function g_l provides the magnitude of the lateral acceleration aimed at centering vehicle i at position x_l.

2.4. Lane changing

The simplest way to handle lane-changing execution (LCE) is by changing the value of x_l in (6) to the center of the target lane, as shown in Algorithm 1. Following this criterion, no additional rules or parameters are needed to model lane-changing maneuvers. We will discuss later on the implications of this criterion.

Although a lane-changing decision (LCD) model determines when the value of x_l changes from one lane to the other, LCE is independent from the LCD model. Therefore, it can be coupled with most existing LCD models, including one developed ad-hoc for the present car-following model and is described in Section 4.

Algorithm 1. Lane changing model

```
if LCD model mandates to change to lane l' then
    x_l ← x_l'//change lanes
end if
```

3. Lateral friction

In this section, we describe the experiments aimed at reproducing lateral friction.

For simplicity, in the experiments presented here and the next two sections, we define the following linear functional forms for $\vec{f}^{\,a}$ and $\vec{f}^{\,l}$:

$$f_{i,k}^{a,y} = g_a(v_i^y(t)) \coloneqq (V - v_i^y(t))c_1 \tag{7}$$

$$f_i^{l,x} = g_l(v_i^x(t), x_i(t) - x_l) \coloneqq -v_i^x(t)k_1 - (x_i(t) - x_l)k_2, \tag{8}$$

In (7), V and c_1 are the same as in the 1D model. In turn k_1 and k_2 in (8) are parameters of the 2D model, measuring the intensity of the response per unit of lateral speed (in units of time^{-1},) and the lateral distance to the center of the lane (in units of time^{-2}), respectively. Note that (8) defines a damped harmonic oscillator around the center of the lane. As such, it can be further specified as critically damped, making k_1 and k_2 dependent on each other, $k_1 = 2\sqrt{k_2}$, and reducing the number of parameters in one.

For the repulsive force, we need to consider that the repulsion generated by a vehicle at one longitudinal meter is not the same as the one generated by a vehicle at one lateral meter. For this reason, we define a scaling factor to convert longitudinal distance into lateral distance. This factor $q(v_i)$ depends on longitudinal speed, and for simplicity we assume that when applied to longitudinal distance makes the effect of distance in any direction comparable. This assumption implies that level curves of the repulsive force's strength under analogous conditions are elliptical. We call this transformation *scaling*. The scaled distance vector $\vec{r}_{i,k}^{\,*}$ between vehicles i and k is defined in (9).

$$\vec{r}_{i,k}^{\,*}(t) = \begin{bmatrix} x_k(t) - x_i(t) \\ \frac{y_k(t) - y_i(t)}{q} \end{bmatrix} = \begin{bmatrix} 1 & 0 \\ 0 & \frac{1}{q} \end{bmatrix} \left(\vec{x}_k(t) - \vec{x}_i(t) \right) \tag{9}$$

If we define $\mathbf{Q} = \begin{bmatrix} 1 & 0 \\ 0 & q \end{bmatrix}$, Eq. (9) can be rewritten as follows:

$$\vec{r}^{*}_{i,k}(t) = \mathbf{Q}^{-1}(\vec{x}_k(t) - \vec{x}_i(t)) \tag{10}$$

For convenience and simplicity, we choose a vector function $\vec{g}_r$ that satisfies the following conditions after scaling: (*i*) it yields a linear response to distance and radial speed difference, (*ii*) vehicles traveling at the same speed and direction do not repel each other if the distance between them, considering every direction, is greater than a constant distance x^* (a parameter of the model), and (*iii*) it generalizes our previous 1D model (i.e., the previous model becomes a particular case of the new one).

Scaled radial speed difference $\Delta\vec{v}^{*}_{i,k}(t)$ is computed by projecting the scaled speed difference to $\hat{r}^{*}_{i,k}(t)$, as in (11). The variable $\hat{r}^{*}_{i,k}(t)$ is the unit vector corresponding to $\vec{r}^{*}_{i,k}(t)$.

$$\Delta\vec{v}^{*}_{i,k}(t) = \mathbf{Q^{-1}}(\vec{v}_k(t) - \vec{v}_i(t)).\ \hat{r}^{*}_{i,k} \tag{11}$$

$$\hat{r}^{*}_{i,k}(t) = \frac{\vec{r}^{*}_{i,k}(t)}{\|\vec{r}^{*}_{i,k}(t)\|} \tag{12}$$

Under our assumptions, $q(v)$ must be such that $x^{*}\cdot q(v)$ equals the zero-repulsion distance $v\tau_r + s_r$ from the 1D model in Eq. (1). Therefore, the scaling factor is defined in (14).

$$x^{*}q(v) = v\tau_r + s_r \tag{13}$$

$$q(v) = \frac{v\tau_r + s_r}{x^{*}} \tag{14}$$

Finally, the repulsive force in (5) is defined according to (15), which satisfies the three conditions previously stated. Note that the direction of the repulsive force needs to be scaled back to the original coordinate system to match the actual direction to vehicle *k*.

$$\vec{f}^{\,r}_{i,k} \coloneqq \mathbf{Q}\hat{r}^{*}_{i,k}(t)\min\{0,\ \Delta\vec{v}^{*}_{i,k}(t)c_2 + (\|\vec{r}^{*}(t)\| - x^{*})c_3,\} \tag{15}$$

Scaling factor q is a dimensionless quantity. Based on (14), q depends on x^*, which is measured in units of distance. One alternative is to consider x^* (or q) to be constant and independent of the speed. By doing this, x^* (or q) would be one of the model's parameters, as proposed above. Another alternative, and possibly a more realistic option, is to consider both x^* and q linear with respect to speed, which would add two parameters to the model.

Distance x^* is non-negative and should not be greater than a few meters; otherwise, friction is possible between streams of vehicles that are too far apart in the lateral direction. From (14), $q \geqslant \frac{s_r}{x^{*}}$. This ratio is intuitively greater than 1. In the following experiments, using realistic parameter values, q is never smaller than 10. Assuming some friction takes place between two neighboring lanes—one at free flow and one completely stopped—q should not be greater than the ratio between the critical longitudinal gap and a standard lateral gap (i.e. on the order of a few tens.) This analysis of the meaning and properties of the 2D parameters of the model can be seen in more detail in Delpiano (2015). Table 1 summarizes all the resulting model's parameters, along with their meaning and units.

A number of traditional (i.e. longitudinal) car-following models, including the one described by (1), consider vehicles as point masses, dealing with headway and spacing rather than time and space gaps. In practice, this assumption does not work equally well in the lateral direction. Vehicle width is frequently comparable in magnitude to the lateral separation between vehicles in adjacent lanes, and this becomes especially relevant at higher speeds. Lane discipline implies that a difference in lateral position between a leader and its follower sharing the same lane does not usually affect their behavior. However, a similar difference in the longitudinal positions between two vehicles in adjacent lanes can determine which vehicle will eventually follow the other after an aggressive lane-changing maneuver. To address this issue, the distance and direction for the purpose of the repulsive force need to be defined by considering the vehicles' width but not its length.

Table 1
Summary of the model's parameters. Five are necessary for the longitudinal dimension, and two for the 2D extension.

Parameter	Meaning	Typical range	Units
V	Free-flow speed	15–35	$m{\cdot}s^{-1}$
c_1	Sensitivity to own speed	0.03–0.1	s^{-1}
c_2	Sensitivity to speed difference*	0–1	s^{-1}
c_3	Sensitivity to spacing	0–1	s^{-2}
s_r	Repulsive force's jam range	10–30	m
τ_r	Repulsive force's sensitivity to speed	0–1	s
k_1	Sensitivity to lateral speed	0–3	s^{-1}
k_2	Sensitivity to distance to lane's center*	0–1	s^{-2}
x^*	Repulsive force's nominal width	1–3	m

* in particular cases, this parameter may be expressed as a function of others.

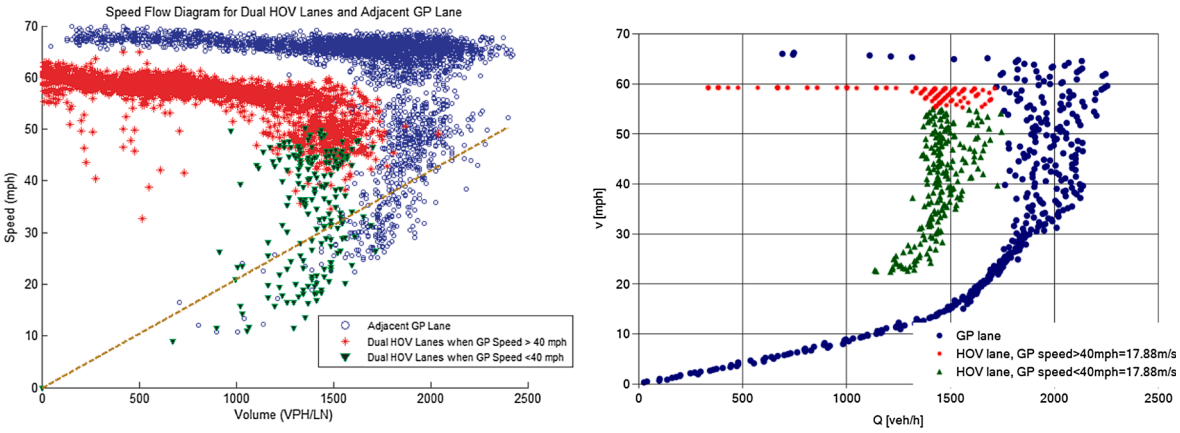

(a) Field measurements. Source: Liu et al. (2011). (b) Simulation results

Fig. 4. Fundamental diagram (flow versus speed) showing the effect of lateral friction. (a) Original situation as reported by Liu et al. (2011) and (b) simulated results using the model proposed.

3.1. The experiment

Lateral friction happens when drivers tend to reduce their speed based on traffic and/or objects adjacent to their traveling lane. Here we replicate the experimental data reported in Liu et al. (2011, site D), in which the slow general-purpose (GP) lanes induce vehicles in the faster HOV lane to reduce their speed despite being in free-flow conditions and lane changes forbidden.

The experimental setup consists of a two-lane, 1 km-long highway segment studied during 1,800 s. Lane 1 is the left lane and plays the role of the HOV lane. Demand on the HOV lane grows linearly from 150 veh/h to 1500 veh/h during the first half, similar to the situation described in Liu et al. (2011). During the second half, the demand stays at 1500 veh/h, which is below capacity. Lane 2 plays the role of the GP lane. Traffic flow in this lane is such that the lane works at capacity with a maximum of 2000 vehicles per hour. The speed on this lane is forcefully and progressively reduced at a rate of 1 m/s every minute, according to Eq. (16), to emulate downstream congestion propagating backward.

$$v_{max} = \max\left\{30 - \frac{t}{60}, 0\right\}\left[\frac{\text{m}}{\text{s}}\right], \tag{16}$$

Parameter x^* was obtained through calibration and is set at 1.9 m. The lane force parameters are $k_1 = 1$ y $k_2 = \frac{1}{4}$ (Delpiano, 2015). The linear model parameters' are $c_1 = \frac{1}{10}$, $c_2 = \frac{33}{64}$, $c_3 = \frac{9}{64}$, $\tau_r = \frac{8}{10}$, and $s_r = \frac{196}{9}$, all of them within a reasonably realistic range. The parameters also meet the condition in (2), thus enabling the model to reproduce traffic instability. Finally, parameter V is set to $30\left[\frac{\text{m}}{\text{s}}\right]$ (68 mph) for the GP lane and $26.5\left[\frac{\text{m}}{\text{s}}\right]$ (60 mph) for the HOV lane to reproduce original free-flow conditions.

Fig. 4a shows the original fundamental diagram (Liu et al., 2011, fig. 7a), and Fig. 4b shows the one resulting from the simulation. The agreement between both diagrams confirms the ability of the proposed model to replicate lateral friction. The less spread exhibited in the simulated fundamental diagram as compared to the original one is mainly due to the absence of driver variability in the simulations. Despite the model being very simple, it is capable of reproducing the main effects qualitatively and to a fairly satisfactory level, even if the results are not numerically exact.

Additional evidence is provided in Fig. 5, which compares the speed measured on both lanes. In the absence of lateral friction, all the points would lay on the horizontal line corresponding to the free flow speed at the HOV lane, i.e. 60 mph.

The model is able to reproduce lateral friction observed in the field. Low speeds on the GP lane force the stream of vehicles on the HOV lane to reduce their speed, despite its relatively low traffic demand and the absence of lane changes.

4. Relaxation

Recall that the relaxation phenomenon describes the situation in which drivers accept very small spacings when entering a freeway, and then gradually increase their spacing to normal levels. As reported in Kim and Coifman (2013), this mechanism induces flows greater than capacity for a short period of time, followed by a lower discharge rate. This drop in discharge rate can be further exacerbated by the capacity drop caused by the voids created by vehicle bounded accelerations (Laval and Daganzo, 2006).

As mentioned earlier, our model captures relaxation naturally. We argue that relaxation begins before the end of the lane-changing maneuver, as a result of a 2D collision avoidance behavior, i.e. the repulsive force $f^r_{i,k}$.

To illustrate this, consider a five-lane, 1000 m long segment from ($y = 0$ to $y = 1000$) with an on-ramp between $y = 400$ and 500 m. Vehicles on the on-ramp merge by centering with respect to an oblique line joining the center of the origin lane at $y = 400$ with the center of the destination lane at $y = 500$, as shown in Fig. 6 (i.e. x_l in Eq. (6) for merging vehicles is made a function of y). This

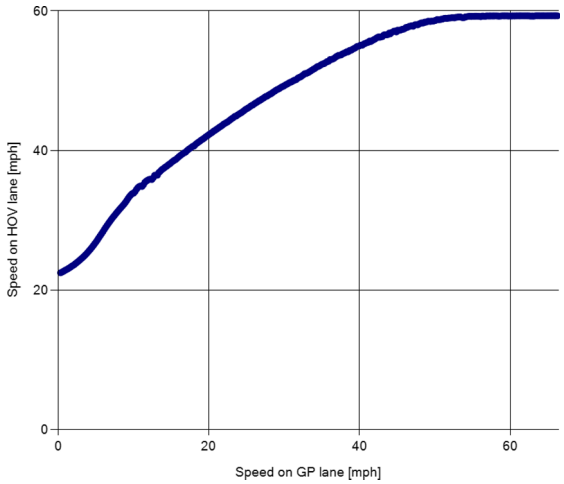

Fig. 5. Speed comparison between HOV and GP lanes in the simulation.

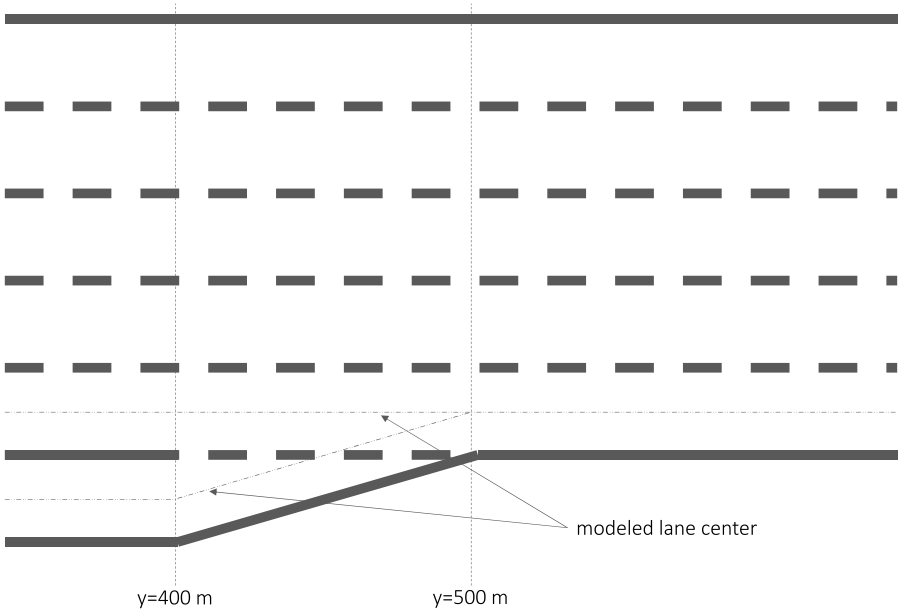

Fig. 6. Schematics of modeled highway segment and on-ramp for capacity drop.

conditions the way in which compulsory lane changes are performed in the bottleneck without the involvement of an LCD model. In this way, we avoid making explicit use of a point bottleneck model, as discouraged by Coifman and Kim (2011).

Traffic demand considering both the mainline and the on-ramp is slightly greater than the capacity of the five-lane segment. The simulation ran for 1800 s. All lane changes were registered, along with their time and location, in order to measure lane-changing rates before and after the capacity drop. Based on Cassidy and Rudjanakanoknad (2005), discretionary lane changes to the left (excluding the on-ramp) were counted between $y = 390$ and $y = 630$ m. Discharge rates were measured at $y = 400$, 500, 800, and 1000.

The functional form of the forces for the car-following model to be used in this experiment is the same as described in Section 3. The modularity of our framework allows us to test different lane-changing models in order to explore the influence of such different approaches on the capacity drop. Specifically, experiments were conducted using the following LCD models: (*i*) a modified version of Gipps (1986) as implemented by simulation software Aimsun (TSS, 2010) with a maximum deceleration (b) of 4.6 $\left[\frac{\text{m}}{\text{s}^2}\right]$, a threshold t_o of 90% of the maximum desired speed in order to make a faster lane desirable, and a threshold t_r of 95% for the maximum desired speed to make a slower lane acceptable; (*ii*) Laval and Leclercq (2008) (using $\tau = 4$ s); and (*iii*) a simple, *ad-hoc* model that triggers a lane-changing maneuver if the target lane would induce in the vehicle a repulsive force which is at most $\delta_r \left[\frac{\text{m}}{\text{s}^2}\right]$ weaker than its current repulsive force, and the new follower would not need to reduce its speed by $d_t \left[\frac{\text{m}}{\text{s}}\right]$ by the time the lane-change is half-

Table 2
Relaxation experiments.

Exp.	LCD Model	Parameters
1	Laval and Leclercq (2008)	$\tau = 4$ s
2	Gipps (1986)	$b = 4.6\left[\frac{\text{m}}{\text{s}^2}\right]$, $t_o = 90\%$, $t_r = 95\%$
3	Social forces, anticipative	$\delta_r = 2.9\left[\frac{\text{m}}{\text{s}^2}\right]$, $d_t = 20\left[\frac{\text{m}}{\text{s}}\right]$

completed. Table 2 synthesizes the experiments to be conducted.

Evidence of the ability of the model to reproduce relaxation and the related symptoms is shown in Figs. 7–9. Fig. 7 shows traffic states at location $y = 550$ and $y = 850$ before the capacity drops, which occurs around 900 s. In the figure, each point represents a traffic state as calculated using Eddie's generalized definitions (Edie, 1963) for time intervals of 10 s and 18 m-long highway segments. Oblique lines in the figure indicate the theoretical fundamental diagram derived from the parameters' values (i.e., in absence of friction, lane changes or other influences) and the approximate one resulting from the experiments.

Fig. 8 shows vehicle trajectories in the target lane for vehicles merging from the on-ramp, after the drop in capacity. Mandatory lane changes (from the on-ramp) are clearly identifiable. Relaxation is also visible: small headways observed immediately after the lane line is crossed by the lane-changing vehicle are progressively increased as the vehicles advance.

Table 3 summarizes the results for each experiment. Drops in capacity were observed, ranging from 3.7 to 8.6%, well within the range reported in the literature (Chung et al., 2007), and consistent with those predicted in theory (Leclercq et al., 2011; Leclercq et al., 2016). Bounded acceleration creates voids that reduce capacity. In turn, aggressive lane-changes give place to gaps that cannot be sustained over time, inducing relaxation. Fig. 9 shows the resulting oblique curves of flow and discretionary lane changes to the left, excluding those from the on-ramp, for experiment 3 as in Cassidy and Bertini (1999, 2005).

All experiments succeeded in reproducing the relaxation phenomenon. Hence, the phenomenon is consistent with the idea of 2D collision avoidance in the context of aggressive lane-changing. Capacity drop and other associated symptoms were also reproduced. The number of discretionary lane changes also evolves according to empirical evidence, where a sudden increase in the number of lane-changes takes place at the same time of the capacity drop (Cassidy and Rudjanakanoknad, 2005; Laval and Daganzo, 2006). Notice that in experiment 2 this is not the case, suggesting that gap acceptance models are unable to capture this fundamental feature of traffic. This failure was expected and is consistent with Daamen et al. (2010).

5. Lateral collision avoidance by autonomous vehicles

Recall that AVs have been involved in lateral collisions due to lane-discipline. The following experiment demonstrates that our proposed framework captures the intricacies of such hazardous situation.

Consider a regular vehicle (RV) traveling on the right lane and an AV traveling on the left lane. Longitudinally, the RV vehicle is slightly ahead of the AV. We refer to this distance as the longitudinal offset between both vehicles. At time $t = 0$, the RV decides to change lanes unaware of the AV, which could cause a collision between both vehicles. In the model, the occurrence of this type of

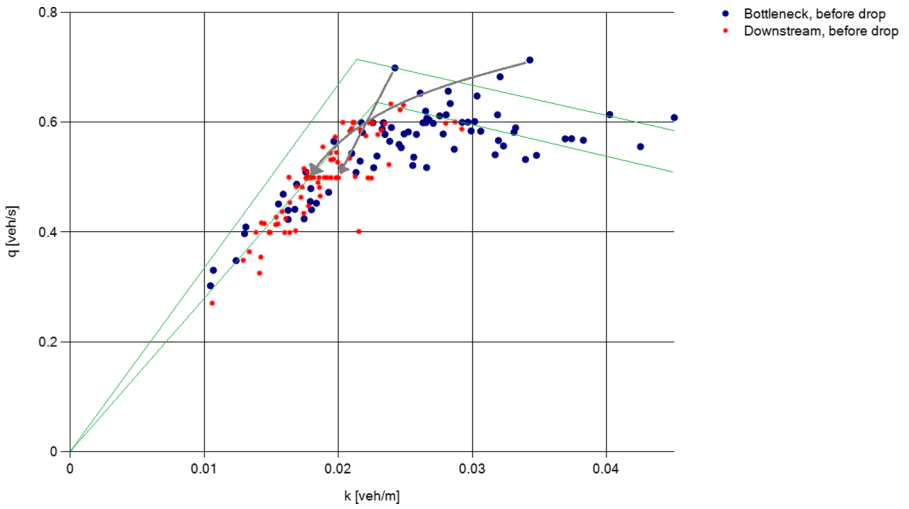

Fig. 7. Fundamental diagram showing out-of-equilibrium traffic states in bottleneck ($y = 550$) and downstream ($y = 850$) before capacity drops. Lines depict theoretical (upper) and practical (lower) fundamental diagram resulting from friction and lane changes. Arrows link traffic states experienced by selected platoons of vehicles at both locations.

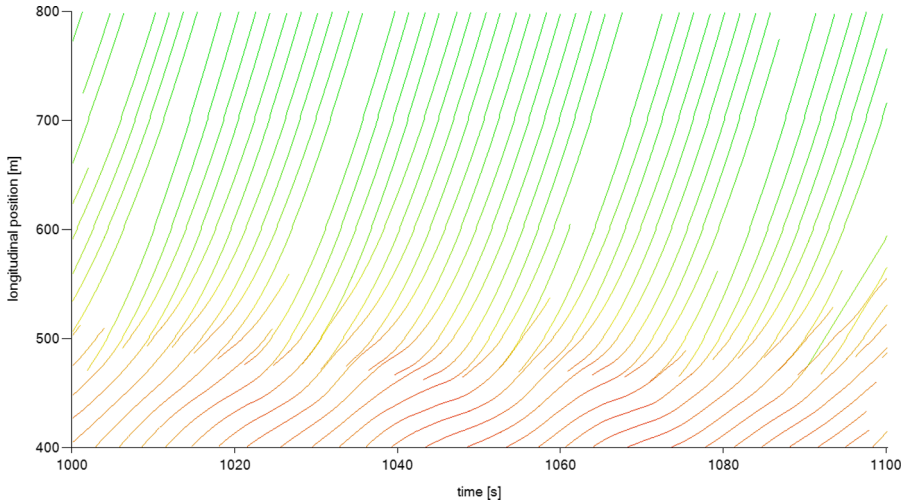

Fig. 8. Vehicle trajectories in lane 2, longitudinal position vs. time. Mandatory lane changes and subsequent relaxation are observed.

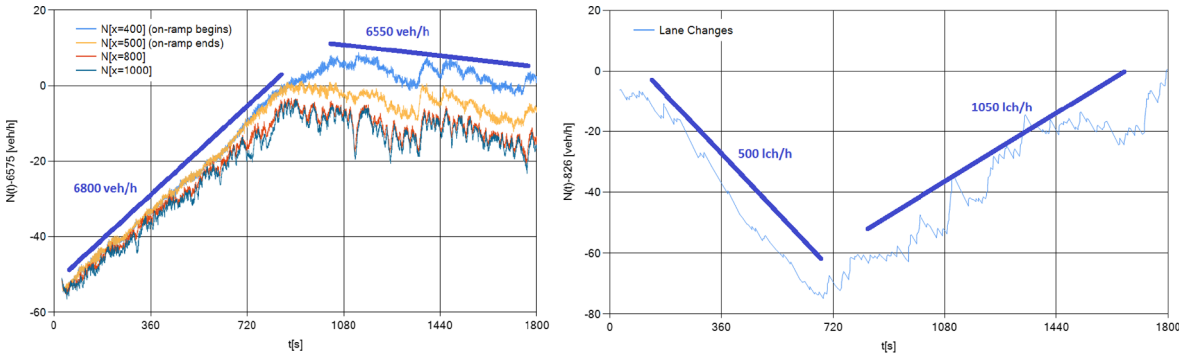

(a) (b)

Fig. 9. Oblique curves of flow and discretionary lane changes to the left between lanes other than on-ramp for experiment 3. Parameter's values were set as follows: $c_1 = \frac{3}{40}$, $c_2 = \frac{93}{160}$, $c_3 = \frac{9}{64}$, $\tau_r = \frac{2}{3}$, $s_r = \frac{220}{9}$, $V = \frac{100}{3}$ per Delpiano et al. (2015), $k_1 = 1$ and $k_2 = \frac{1}{4}$ as in the previous experiment, $x^* = 1.6$, $\delta_r = 2.9$, and $d_t = 20$. The last three parameters were calibrated.

Table 3
Capacity drop results.

	flow $\left[\frac{veh}{h}\right]$			discr. lane changes $\left[\frac{1}{h}\right]$		
Exp.	Before	After	Change	Before	After	Change
1	7100	6800	−4.2%	530	1100	107.5%
2	7000	6400	−8.6%	400	90	-77.5%
3	6800	6550	−3.7%	500	1050	110.0%

accident caused by such a maneuver depends on the formulation of the repulsive (5) and lane forces (6).

In this experiment, we keep the functional forms for the forces as defined in Section 3 and the parameters used in Section 4, except for the value of x^*. That is, we change the scaling factor $q(v_i)$ in such a way that higher values of x^* yield a smaller scaling factor for the same velocity. For a given value of x^*, we are interested in looking for the minimum longitudinal offset at $t = 0$ needed to prevent vehicles from colliding. Formulations as well as all the remaining parameters are set as in the previous experiment. Lane width is 3.6 m and both vehicles are 1.7 m wide and 4.65 m long.

Fig. 10 shows the results of this experiment. If $x^* = 1.6$ or 1.9, as in previous experiments, an initial longitudinal offset of at least 35 and 20 cm, respectively, are needed to avoid collision. Smaller values of x^* require a longer initial longitudinal offset.

Fig. 11 sketches a single lane-changing maneuver when the initial longitudinal offset at $t = 0$ is 2 m and $x^* = 1.9$ m. The center of the left lane, on which the AV is traveling, corresponds to $x = 0$, while the center of the right lane where the RV is traveling

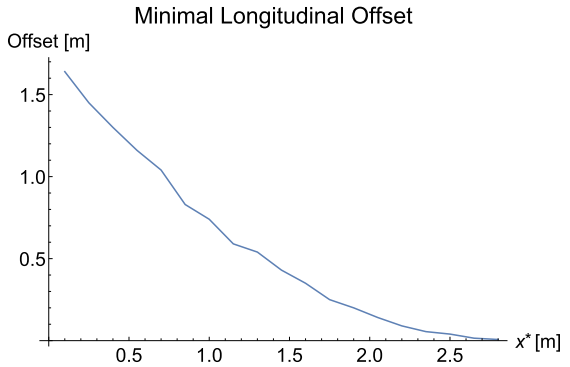

Fig. 10. Minimal initial longitudinal offset required to avoid collision, given a lane-changing vehicle unaware of another vehicle in the adjacent lane, for different values of x^*.

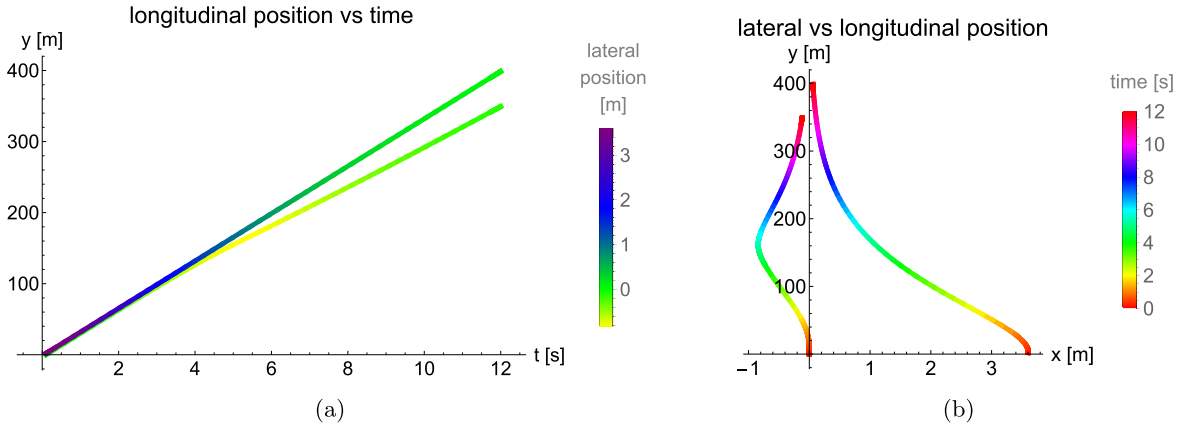

Fig. 11. Evolution of lateral and longitudinal positions of vehicles during a hazardous lane-changing maneuver.

corresponds to $x = 3.6$.

The graph on the left (a) is a conventional time-space diagram showing the trajectories for both vehicles. The lateral position is represented by color. The graph on the right (b) is the same maneuver in 2D space. The curves in the graph represent the 2D trajectories of both vehicles. In this case, time is represented by color. Note how the AV responds to the unexpected maneuver of the RV by moving laterally to the left and reducing its speed. All these are the results of the repulsive forces acting over the AV, and allow it to successfully avoid the incoming RV and settles behind it.

An alternative non-linear formulation for the response of the repulsive force to distance was tested. In this case, the term $(\|\vec{r}^*(t)\| - x^*)c_3$ in Eq. (15) is replaced by a non-linear function. The expression for the repulsive force is shown in (17).

$$\vec{f}^{\,r}_{i,k} = \mathbf{Q}\hat{r}^*_{i,k}(t)\min\left\{0,\ \Delta\vec{v}^*_{i,k}(t)c_2 + x^*c_3\log\frac{\|\vec{r}^*(t)\|}{x^*}\right\}. \tag{17}$$

As it happens with the original term, if $\|\vec{r}^*(t)\| = x^*$, the new term in (17) also becomes zero and its derivative with respect to distance at that point is c_3. The formulation also meets the requirement that the closer the vehicles are, the faster the repulsive force grows. It was found that all collisions were avoided with x^* as low as 97 cm.

6. Discussion

We proposed a two-dimensional (2D) microscopic traffic model by considering the lateral dimension in addition to the longitudinal one. The model contributes to the understanding of (*i*) the lateral friction often observed in HOV lanes, (*ii*) the relaxation phenomenon near congested merge bottlenecks, (*iii*) hazardous lane changing.

Our results show that both lateral friction and relaxation are mostly explained by the repulsive force, confirming that this force can be viewed as a 2D collision avoidance mechanism. These results also highlight the importance of considering lane-changing as a non-instantaneous process. In turn, no *ad-hoc* rules were needed to reproduce these effects. These rules are oftentimes needed in 1D models.

In this specific implementation, we adopted a number of assumptions. For example, we assumed linear responses to stimuli for most of our experiments. Linear responses are known to be an oversimplification allowing for collisions in specific situations. We

believe, however, that they are enough for illustrative purposes, while keeping the focus on the effect of the 2D formulation. We also verified that a non-linear response to lateral distance better represents lateral collision avoidance mechanisms due to aggressive, distracted lane-changing maneuvers. Likewise, the fact that the repulsive force is induced by downstream vehicles only and equally, captures in general the anisotropy of traffic, but could be fine-tuned to better capture the subtleties of interaction between adjacent drivers.

Our results suggest that the proposed 2D approach is suitable to model autonomous vehicles, and that the occurrence of lateral collisions is governed by the lane and repulsive forces introduced here. This means that safe implementation of AV technologies should carefully consider the formulation of their responses to lateral stimuli. In particular, a value of x^* higher than 2.5 m was needed to avoid all possible collisions in Section 5 with a linear response to lateral distance. This would cause repulsion from almost any neighboring vehicle. Therefore, a non-linear response seems reasonable for a driving that is at the same time efficient and safe.

Further research is advised on the formulation of the forces. Topics include but are not limited to study (*i*) whether the lane force should be linear or not, or even if it should be the same for both lane-changing execution and lane centering; (*ii*) the addition of stochastic terms and/or parameters in the formulation to account either for customized AVs, those from different manufacturers, or regular vehicle drivers variability; (*iii*) the relationship between scaling and velocity, for example, if the lateral dimension should also be scaled, or $q(v)$ be non-linear, etc.

The research presented here is helpful in modeling, understanding, and replicating features of human drivers in traffic in the lateral dimension. We consider that this understanding may be key to improving autonomous driving algorithms, to make them both efficient and friendly to passengers as well as people in neighboring vehicles.

This is true not only in a hypothetical future of coordinated, autonomous-only traffic, but especially relevant when streets are shared by both types of drivers and by different designs of autonomous driving algorithms. While technology can easily outperform human reaction time and accuracy, an autonomous vehicle that keeps very short distances or centers too strictly (e.g., when overtaking at high speeds) can baffle its passengers and neighboring human drivers, thus affecting traffic efficiency and even safety.

References

Bando, M., Hasebe, K., Nakayama, A., Shibata, A., Sugiyama, Y., 1995. Dynamical model of traffic congestion and numerical simulation. Phys. Rev. E 51, 1035–1042. https://doi.org/10.1103/PhysRevE.51.1035.

Bellem, H., Thiel, B., Schrauf, M., Krems, J.F., 2018. Comfort in automated driving: An analysis of preferences for different automated driving styles and their dependence on personality traits. Transp. Res. Part F: Traffic Psychol. Behav. 55, 90–100. https://doi.org/10.1016/j.trf.2018.02.036. http://www.sciencedirect.com/science/article/pii/S1369847817301535.

California Department of Motor Vehicles, 2018. Report of Traffic Collision Involving an Autonomous Vehicle (OL 316). https://www.dmv.ca.gov/portal/dmv/detail/vr/autonomous/autonomousvehol316+.

Calvi, A., 2015. Does roadside vegetation affect driving performance?: Driving simulator study on the effects of trees on drivers speed and lateral position. Transp. Res. Rec.: J. Transp. Res. Board 2518, 1–8. https://doi.org/10.3141/2518-01. http://trrjournalonline.trb.org/doi/10.3141/2518-01.

Case, H.W., Hulbert, S.F., Mount, G.E., Brenner, R., 1953. Effect of a roadside structure on the lateral placement of motor vehicles. In: Highway Research Board Proceedings, . http://trid.trb.org/view.aspx?id=116452.

Cassidy, M., Bertini, R., 1999. Some traffic features at freeway bottlenecks. Transp. Res. Part B: Methodol. 33B, 25–42. http://www.scopus.com/inward/record.url?eid=2-s2.0-0032599748&partnerID=40&md5=7734bd7e9b7e2ecfb4f724aeea9e210f.

Cassidy, M., Rudjanakanoknad, J., 2005. Increasing the capacity of an isolated merge by metering its on-ramp. Transp. Res. Part B: Methodol. 39, 896–913. https://doi.org/10.1016/j.trb.2004.12.001. http://www.sciencedirect.com/science/article/pii/S0191261505000044.

Chen, D., Ahn, S., Chitturi, M., Noyce, D.A., 2017. Towards vehicle automation: roadway capacity formulation for traffic mixed with regular and automated vehicles. Transp. Res. Part B: Methodol. 100, 196–221.

Chen, F., Song, M., Ma, X., Zhu, X., 2019. Assess the impacts of different autonomous trucks lateral control modes on asphalt pavement performance. Transp. Res. Part C: Emerg. Technol. 103, 17–29. https://doi.org/10.1016/j.trc.2019.04.001. http://www.sciencedirect.com/science/article/pii/S0968090X18312646.

Chitturi, M., Benekohal, R., 2005. Effect of lane width on speeds of cars and heavy vehicles in work zones. Transp. Res. Rec.: J. Transp. Res. Board 1920, 41–48. https://doi.org/10.3141/1920-05.

Chung, K., Rudjanakanoknad, J., Cassidy, M.J., 2007. Relation between traffic density and capacity drop at three freeway bottlenecks. Transp. Res. Part B: Methodol. 41, 82–95. https://doi.org/10.1016/j.trb.2006.02.011. http://www.sciencedirect.com/science/article/pii/S0191261506000397.

Coifman, B., Kim, S., 2011. Extended bottlenecks, the fundamental relationship, and capacity drop on freeways. Transp. Res. Part A: Policy Pract. 45, 980–991. https://doi.org/10.1016/j.tra.2011.04.003. http://www.sciencedirect.com/science/article/pii/S0965856411000619.

Daamen, W., Loot, M., Hoogendoorn, S.P., 2010. Empirical analysis of merging behavior at freeway on-ramp. Transp. Res. Rec.: J. Transp. Res. Board 2188, 108–118. https://doi.org/10.3141/2188-12.

Delis, A.I., Nikolos, I.K., Papageorgiou, M., 2015. Macroscopic traffic flow modeling with adaptive cruise control: Development and numerical solution. Comput. Math. Appl. 70, 1921–1947.

Delpiano, R., 2015. Modelo Microscópico de Tráfico en Dos Dimensiones Basado en Fuerzas Sociales. PhD's thesis. Pontificia Universidad Católica de Chile. doi:https://doi.org/10.13140/RG.2.2.22576.05126.

Delpiano, R., Laval, J.A., Coeymans, J.E., Herrera, J.C., 2015. The kinematic wave model with finite decelerations: a social force car-following model approximation. Transp. Res. Part B: Methodol. https://doi.org/10.1016/j.trb.2014.10.005.

Edie, L.C., 1963. Discussion of traffic stream measurements and definitions. Port of New York Authority.

Ghiasi, A., Hussain, O., Qian, Z.S., Li, X., 2017. A mixed traffic capacity analysis and lane management model for connected automated vehicles: a markov chain method. Transp. Res. Part B: Methodol. 106, 266–292.

Gipps, P., 1986. A model for the structure of lane-changing decisions. Transp. Res. Part B: Methodol. 20, 403–414. doi: 16/0191-2615(86)90012-3. http://www.sciencedirect.com/science/article/pii/0191261586900123.

Gunay, B., 2007. Car following theory with lateral discomfort. Transp. Res. Part B: Methodol. 41, 722–735. https://doi.org/10.1016/j.trb.2007.02.002. http://www.sciencedirect.com/science/article/pii/S0191261507000161.

Helbing, D., Molnár, P., 1995. Social force model for pedestrian dynamics. Phys. Rev. E 51, 4282–4286. https://doi.org/10.1103/PhysRevE.51.4282.

Helbing, D., Tilch, B., 1998. Generalized force model of traffic dynamics. Phys. Rev. E 58, 133–138. https://doi.org/10.1103/PhysRevE.58.133.

Helly, W., 1959. Simulation of bottlenecks in single-lane traffic flow. In: Proceedings of the Syposium on Theory of Traffic Flow, pp. 207–238.

Jin, S., Wang, D., Tao, P., Li, P., 2010. Non-lane-based full velocity difference car following model. Physica A 389, 4654–4662. doi: 16/j.physa.2010.06.014. http://www.sciencedirect.com/science/article/pii/S0378437110005042.

Jin, S., Wang, D.-H., Yang, X.-R., 2011. Non-lane-based car-following model with visual angle information. Transp. Res. Rec.: J. Transp. Res. Board 2249, 7–14.

https://doi.org/10.3141/2249-02.
Kanagaraj, V., Treiber, M., 2018. Self-driven particle model for mixed traffic and other disordered flows. Physica A 509, 1–11. https://doi.org/10.1016/j.physa.2018.05.086. http://www.sciencedirect.com/science/article/pii/S0378437118306356.
Katrakazas, C., Quddus, M., Chen, W.-H., Deka, L., 2015. Real-time motion planning methods for autonomous on-road driving: State-of-the-art and future research directions. Transp. Res. Part C: Emerg. Technol. 60, 416–442. https://doi.org/10.1016/j.trc.2015.09.011. http://www.sciencedirect.com/science/article/pii/S0968090X15003447.
Kesting, A., Treiber, M., Schönhof, M., Helbing, D., 2008. Adaptive cruise control design for active congestion avoidance. Transp. Res. Part C: Emerg. Technol. 16, 668–683.
Kim, S., Coifman, B., 2013. Freeway on-ramp bottleneck activation, capacity and the fundamental relationship. Procedia – Soc. Behav. Sci. 80, 698–716. https://doi.org/10.1016/j.sbspro.2013.05.037. http://www.sciencedirect.com/science/article/pii/S1877042813010069.
Laval, J.A., Daganzo, C.F., 2006. Lane-changing in traffic streams. Transp. Res. Part B: Methodol. 40, 251–264. https://doi.org/10.1016/j.trb.2005.04.003. http://www.sciencedirect.com/science/article/pii/S019126150500055X.
Laval, J.A., Leclercq, L., 2008. Microscopic modeling of the relaxation phenomenon using a macroscopic lane-changing model. Transp. Res. Part B: Methodol. 42, 511–522. doi: 16/j.trb.2007.10.004. http://www.sciencedirect.com/science/article/pii/S0191261507001312.
Le Vine, S., Zolfaghari, A., Polak, J., 2015. Autonomous cars: the tension between occupant experience and intersection capacity. Transp. Res. Part C: Emerg. Technol. 52, 1–14. https://doi.org/10.1016/j.trc.2015.01.002. http://www.sciencedirect.com/science/article/pii/S0968090X15000042.
Leclercq, L., Knoop, V.L., Marczak, F., Hoogendoorn, S.P., 2016. Capacity drops at merges: new analytical investigations. Transp. Res. Part C: Emerg. Technol. 62, 171–181. https://doi.org/10.1016/j.trc.2015.06.025. http://www.sciencedirect.com/science/article/pii/S0968090X15002405.
Leclercq, L., Laval, J.A., Chiabaut, N., 2011. Capacity drops at merges: an endogenous model. Transp. Res. Part B: Methodol. 45, 1302–1313. https://doi.org/10.1016/j.trb.2011.05.007. http://www.sciencedirect.com/science/article/pii/S0191261511000579.
Liu, X., Schroeder, B., Thomson, T., Wang, Y., Rouphail, N., Yin, Y., 2011. Analysis of operational interactions between freeway managed lanes and parallel, general purpose lanes. Transp. Res. Rec.: J. Transp. Res. Board 2262, 62–73. https://doi.org/10.3141/2262-07. http://trrjournalonline.trb.org/doi/10.3141/2262-07.
Mahmassani, H.S., 2016. 50th Anniversary invited article autonomous vehicles and connected vehicle systems: flow and operations considerations. Transp. Sci. 50, 1140–1162. https://doi.org/10.1287/trsc.2016.0712.
Maurya, A., 2011. Comprehensive approach for modeling of traffic streams with no lane discipline. In: Proceedings of the 2nd International Conference on Models and Technologies for Intelligent Transportation Systems 071. http://www.mech.kuleuven.be/MT-ITS2011/downloads/Abstracts/071, A. Maurya, Comprehensive Approach for Modeling of Traffic Streams with No Lane Discipline.pdf.
May, A.D., 1959. Friction concept of traffic flow. Highway. In: Research Board Proceedings, . http://trid.trb.org/view.aspx?id=117080.
Moridpour, S., Sarvi, M., Rose, G., 2010. Modeling the lane-changing execution of multiclass vehicles under heavy traffic conditions. Transp. Res. Rec.: J. Transp. Res. Board 2161, 11–19. https://doi.org/10.3141/2161-02. http://trb.metapress.com/openurl.asp?genre=article&id=doi:10.3141/2161-02.
Reece, D.A., Shafer, S.A., 1993. A computational model of driving for autonomous vehicles. Transp. Res. Part A: Policy Pract. 27, 23–50. https://doi.org/10.1016/0965-8564(93)90014-C. http://www.sciencedirect.com/science/article/pii/096585649390014C.
Schönauer, R., Stubenschrott, M., Huang, W., Rudloff, C., Fellendorf, M., 2012. Modeling concepts for mixed traffic. Transp. Res. Rec.: J. Transp. Res. Board 2316, 114–121. https://doi.org/10.3141/2316-13.
Shladover, S., Su, D., Lu, X.-Y., 2012. Impacts of cooperative adaptive cruise control on freeway traffic flow. Transp. Res. Rec.: J. Transp. Res. Board 63–70.
Talebpour, A., Mahmassani, H.S., 2016. Influence of connected and autonomous vehicles on traffic flow stability and throughput. Transp. Res. Part C: Emerg. Technol. 71, 143–163.
Talebpour, A., Mahmassani, H.S., Hamdar, S.H., 2017. Effect of information availability on stability of traffic flow: percolation theory approach. Transp. Res. Procedia 23, 81–100. https://doi.org/10.1016/j.trpro.2017.05.006.
Tampère, C.M.J., 2004. Human-kinetic multiclass traffic flow theory and modelling: with application to advanced driver assistance systems in congestion. Ph.D. thesis Netherlands TRAIL Research School Delft, the Netherlands.
Taragin, A., 1955. Driver behavior as affected by objects on highway shoulders. In: Highway Research Board Proceedings.
Treiber, M., Hennecke, A., Helbing, D., 2000. Congested traffic states in empirical observations and microscopic simulations. Phys. Rev. E 62, 1805–1824. https://doi.org/10.1103/PhysRevE.62.1805.
TSS, T.S.S., 2010. Microsimulator and Mesosimulator Aimsun 6.1 User's Manual. TSS-Transport Simulation Systems.
Van Arem, B., Van Driel, C.J., Visser, R., 2006. The impact of cooperative adaptive cruise control on traffic-flow characteristics. IEEE Trans. Intell. Transp. Syst. 7, 429–436.
Yang, D., Zhu, L., Ran, B., Pu, Y., Hui, P., 2016. Modeling and analysis of the lane-changing execution in longitudinal direction. IEEE Trans. Intell. Transp. Syst. PP, 1–9. https://doi.org/10.1109/TITS.2016.2542109.
Zhang, T., Tao, D., Qu, X., Zhang, X., Lin, R., Zhang, W., 2019. The roles of initial trust and perceived risk in publics acceptance of automated vehicles. Transp. Res. Part C: Emerg. Technol. 98, 207–220. https://doi.org/10.1016/j.trc.2018.11.018. http://www.sciencedirect.com/science/article/pii/S0968090X18308398.
Zhang, T., Tao, D., Qu, X., Zhang, X., Zeng, J., Zhu, H., Zhu, H., 2020. Automated vehicle acceptance in China: social influence and initial trust are key determinants. Transp. Res. Part C: Emerg. Technol. 112, 220–233. https://doi.org/10.1016/j.trc.2020.01.027. http://www.sciencedirect.com/science/article/pii/S0968090X19312537.